Quantum wires, quantum dots, and other low-dimensional systems

Conference paper
UDC 535.372
DOI: https://doi.org/10.18721/JPM.191.109

Photoluminescence control of WSe_2 monolayers integrated with plasmon nanobumps via strain engineering

A.V. Nikolaeva [1,2]✉, M.A. Anikina [1,2], D.V. Pavlov [3], F.M. Maksimov [1,4], A. Kuznetsov [1], V.M. Kondratev [1,2], V.A. Sharov [2,5], A.A. Kuchmizhak [3,6], A.D. Bolshakov [1,2,7]

[1] Moscow Institute of Physics and Technology (National Research University), Moscow, Russia;
[2] Alferov University, St. Petersburg, Russia;
[3] Institute of Automation and Control Processes FEB RAS, Vladivostok, Russia;
[4] Russian Quantum Center, Moscow, Russia;
[5] Ioffe Institute, St. Petersburg, Russia;
[6] Far Eastern Federal University, Vladivostok, Russia;
[7] St. Petersburg State University, St. Petersburg, Russia
✉ nikalex2000@bk.ru

Abstract. This work presents a hybrid system for photoluminescence control, consisting of a tungsten diselenide monolayer (1L-WSe_2) integrated with an array of plasmonic gold nanobumps fabricated by femtosecond laser printing. This technique allows precise tuning of the plasmonic resonance in these structures by controlling their geometry. It is shown that this integration provides a dual mechanism for enhancing and controlling photoluminescence (PL). First, the plasmonic resonance significantly amplifies the PL emission near the nanobump due to exciton-plasmon interaction. Second, the deformation of the WSe_2 monolayer on the nanobump leads to a red shift of the PL peak, resulting from modification of the bandgap. A key feature of this system is the ability to control the spectrum by selecting the pump wavelength: changing the excitation energy affects the correlation between the neutral exciton (X^0) and the low-energy dark exciton/trion ($X^{D/T}$) states. Low-temperature microspectroscopy further revealed a deformation-induced redistribution of intensity from the neutral exciton (X^0) to low-energy states, including the dark exciton/trion complex ($X^{D/T}$). These results establish a foundation for a platform of spectrally tunable light sources based on hybrid exciton-plasmon-strain interactions, which offers a pathway for the advancement of nanophotonics and the development of next-generation optoelectronic devices.

Keywords: WSe_2, emitter, nanobump, photoluminescence

Funding: Ministry of Science and Higher Education of the Russian Federation (Grant FSRM-2026-0004, project FSMG-2025-0005); Saint-Petersburg State University (research project 122040800254-4).

Citation: Nikolaeva A.V., Anikina M.A., Pavlov D.V., Maksimov F.M., Kuznetsov A., Kondratev V.M., Sharov V.A., Kuchmizhak A.A., Bolshakov A.D., Photoluminescence control of WSe_2 monolayers integrated with plasmon nanobumps via strain engineering, St. Petersburg State Polytechnical University Journal. Physics and Mathematics. 19 (1.1) (2026) 56–63. DOI: https://doi.org/10.18721/JPM.191.109

Конференционная статья
УДК 535.372
DOI: https://doi.org/10.18721/JPM.191.109

Управление фотолюминесценцией монослоев WSe_2, интегрированных с плазмонными нанобампами, методом деформационной инженерии

А.В. Николаева [1,2]✉, М.А. Аникина [1,2], Д.В. Павлов [3], Ф.М. Максимов [1,4], А. Кузнецов [1], В.М. Кондратьев [1,2], В.А. Шаров [2,5], А.А. Кучмижак [3,6], А.Д. Большаков [1,2,7]

[1] Московский физико-технический институт (национальный исследовательский университет), Москва, Россия;

[2] Академический университет им. Ж.И. Алфёрова РАН, Санкт-Петербург, Россия;

[3] Институт автоматики и процессов управления ДВО РАН, г. Владивосток, Россия;

[4] Российский квантовый центр, Москва, Россия;

[5] Физико-технический институт им. А.Ф. Иоффе РАН, Санкт-Петербург, Россия;

[6] Дальневосточный федеральный университет, г. Владивосток, Россия;

[7] Санкт-Петербургский государственный университет, Санкт-Петербург, Россия

✉ nikalex2000@bk.ru

Аннотация. В данной работе представлена гибридная система для управления фотолюминесценцией, состоящая из монослоя диселенида вольфрама (WSe_2), интегрированного с массивами плазмонных золотых нанобампов, изготовленных методом фемтосекундной лазерной печати, позволяющей точно настраивать плазмонный резонанс таких структур путём контроля их геометрии. Показано, что такая интеграция обеспечивает двойной механизм усиления и управления фотолюминесценцией (ФЛ). Во-первых, плазмонный резонанс значительно усиливает излучение ФЛ в области нанобампа за счёт экситон-плазмонного взаимодействия. Во-вторых, деформация монослоя WSe_2 на нанобампе приводит к смещению пика в спектре ФЛ, что является следствием модификации ширины запрещённой зоны. Ключевой особенностью системы является возможность активного управления спектром путём выбора длины волны накачки: изменение энергии возбуждения влияет на соотношение между состояниями нейтрального экситона (X^0) и низкоэнергетического тёмного экситона/триона ($X^{D/T}$). Низкотемпературная микроспектроскопия дополнительно выявила вызванное деформацией перераспределение интенсивности от нейтрального экситона (X^0) к низкоэнергетическим состояниям, включая комплекс тёмного экситона/триона ($X^{D/T}$). Полученные результаты создают основу для платформы спектрально перестраиваемых источников света на базе гибридных экситон-плазмон-деформационных взаимодействий, что имеет значение для развития нанофотоники и разработки оптоэлектронных устройств нового поколения.

Ключевые слова: WSe_2, эмиттер, фотолюминесценция

Финансирование: Министерство науки и высшего образования Российской Федерации (грант FSRM-2026-0004, проект FSMG-2025-0005); Санкт-Петербургский государственный университет (исследовательский проект 122040800254-4).

Ссылка при цитировании: Николаева А.В., Аникина М.А., Павлов Д.В., Максимов Ф.М., Кузнецов А., Кондратьев В.М., Шаров В.А., Кучмижак А.А., Большаков А.Д. Управление фотолюминесценцией монослоев WSe_2, интегрированных с плазмонными нанобампами, методом деформационной инженерии // Научно-технические ведомости СПбГПУ. Физико-математические науки. 2026. Т. 19. № 1.1. С. 56–63. DOI: https://doi.org/10.18721/JPM.191.109

Introduction

Two-dimensional materials, particularly monolayer transition metal dichalcogenides (TMDC) like MoS_2, WS_2, $MoSe_2$ are ideal for optoelectronics due to their direct bandgap and strong excitonic effects [1 – 3]. The strategy for enhancing material functionality through hybridization with nanostructures is well-established in fields such as sensor technology, which widely employs carbon nanomaterials for signal transduction [4].

A promising approach to overcome the inherent limitations of two-dimensional materials is their integration with nanostructured surfaces. Of particular interest in this context are metallic nanostructures that support plasmonic resonances, the spectral position of which can be precisely tuned by tailoring their geometry. A significant advancement in this field is the development of the femtosecond laser printing method for such plasmonic elements fabrication [5, 6]. In contrast to nanostructured surfaces obtained via complex and costly lithography and etching techniques, laser printing offers a pathway to produce similar structures using an accessible and scalable technology.

This work presents a study of a hybrid system based on a tungsten diselenide monolayer (1L-WSe_2) integrated with gold plasmonic nanobumps (Au-nanobumps). This configuration not only provides significant photoluminescence enhancement through resonant exciton-plasmon interaction but also enables control over the spectral characteristics of the system achieved by modifying the bandgap of the two-dimensional material via its deformation on the nanoscale relief of the nanostructure.

Materials and Methods

In our work, WSe_2 monolayers were obtained using a mechanical exfoliation method and transferred to a target substrate with Au-nanobumps using a custom transfer system based on tsc2 h_q graphene (HQ Graphene, Netherlands). In this transfer method, crystal layers are exfoliated onto the surface of adhesive tape and then deposited onto a polydimethylsiloxane (PDMS) polymer film supported by a glass substrate. Subsequently, the monolayers are transferred from this "stamp" to the target substrate using a dry transfer technique: the polymer film is brought into contact with the substrate and then peeled away, leaving the layers on the substrate surface. During this process, the target substrate is heated to a temperature between 60°C and 100°C, and the contact time between the crystalline monolayers on the polymer film and the substrate is maintained for 2–4 minutes.

The Au-nanobumps metasurface was fabricated by a combination of inexpensive and scalable magnetron sputtering of thin Au films with a direct fs-laser printing technique. First, a gold film with a thickness of 50 nm was coated over a glass substrate using magnetron deposition. Then, laser patterning of the glass-supported Au films was carried out using $\approx$ 200 fs second-harmonic (λ = 515 nm) pulses generated by a regeneratively amplified Yb:KGW laser system (Pharos, Light Conversion) at 50 kHz repetition rate. A computer-driven nanopositioning platform (ANT130XY, Aerotech) ensured precise movement of the sample surface with respect to the laser focal spot, allowing each pulse to form isolated nanobumps arranged into a square-shaped lattice with a period (Λ) defined by the sample scanning speed.

The nanobump arrays fabricated under these conditions are shown in Fig. 1, *a*, with each row corresponding to a specific laser pulse power, expressed as a percentage of the maximum (100% = 2 nJ). Fig. 1, *b* quantifies the empirical linear dependence between laser pulse power and nanobump height, demonstrating that increased energy produces taller nanostructures. Furthermore, each periodic array (with periods of 3, 5, and 10 μm) exhibits a distinct plasmonic resonance, the spectral position of which depends on the bump height, as shown in Fig. 1, *c*.

Using these techniques, we successfully fabricated a hybrid sample consisting of a monolayer WSe_2 integrated with an array of Au nanobumps.

Results and Discussion

Optical characterization of the hybrid structure was performed via Raman and photoluminescence (PL) microspectroscopy using a Horiba LabRAM HR 800 spectrometer (Horiba Scientific, Japan) equipped with a 532 nm diode-pumped solid-state laser.

Fig. 2, *a* shows an optical image of a WSe_2 flake transferred onto a substrate patterned with a periodic array of Au-nanobumps (mean height: 147 nm, base diameter: 364 nm), fabricated

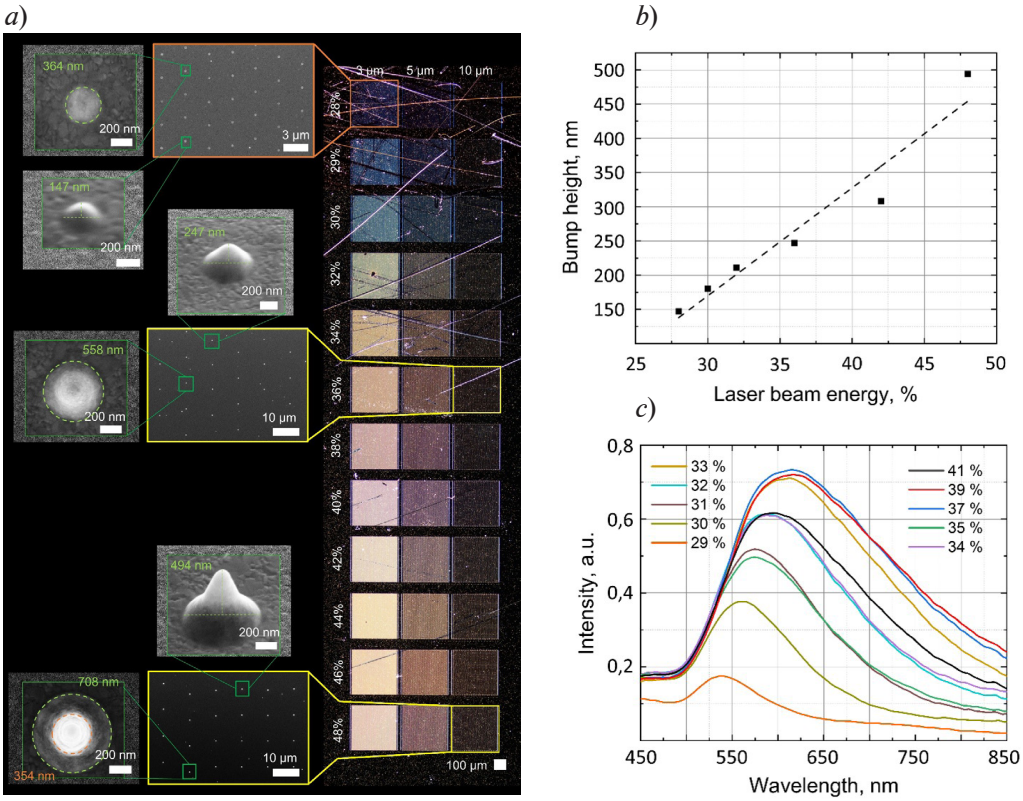

Fig. 1. Au-nanobumps: SEM (left) and optical (right) images of nanobump arrays with periods of 3, 5 and 10 μm (*a*); dependence of the Au-nanobump height on the laser pulses of different output, expressed as a percentage, where 100% corresponds to 2 nJ (*b*); dark-field scattering spectra of Au-nanobump arrays as a function of laser pulses of different output, expressed as a percentage (*c*)

via femtosecond laser printing at a pulse energy of 0.58 nJ (29% of maximum output). The corresponding atomic force microscopy (AFM) topography of this region is presented in Fig. 2, *b*. The flake comprises two distinct thickness domains: a monolayer (1L) and a bilayer (2L) region. AFM analysis demonstrates conformal coverage of the nanostructures, with the flake adopting a tensile, tent-like morphology over each nanobump. Notably, the formation of pronounced folds in the inter-bump regions is enhanced within the bilayer region. The substrate also exhibits a distribution of polydisperse golden nanoparticles (Au-nanoparticles), which are byproducts of the laser fabrication process.

Raman mapping of area *R* (Fig. 2, *a*, *c*) was performed to distinguish the mono- and bilayer regions of WSe_2. The bilayer (2L-WSe_2) region shows a significantly enhanced integrated Raman intensity compared to the monolayer (1L-WSe_2) (Fig. 2, *d*). Furthermore, the spatial boundary is corroborated by a systematic shift in the A'_1 peak position, where the bilayer region exhibits a distinct downshift of several cm^{-1} (Fig. 2, *c*). In the 2L-WSe_2 region, particularly at folds and in the deformed area under the nanobump, a significant enhancement of the integrated Raman scattering intensity is observed. Specifically, in addition to the primary optical modes (A'_1, E') the intensity of the second-order modes at 311 cm^{-1}, 376 cm^{-1}, and 397 cm^{-1} increases. In contrast, these modes are indistinguishable from the noise level in the undeformed monolayer region.

PL mapping across the 1L-WSe_2 region, from the planar area to the Au-nanobump apex (Fig. 3, *b*), along with the AFM map (Fig. 3, *a*) and corresponding spectra (Fig. 3, *d*), reveals two primary strain-dependent effects. First, the PL intensity increases significantly near the Au-nanobump. This enhancement results from a combination of exciton localization, which suppresses non-radiative recombination pathways, and the plasmonic nanoantenna effect of the gold nanostructure, which amplifies the local electromagnetic field. Moreover, the PL peak exhibits a red shift of several nanometers under tensile strain, consistent with a reduction in the direct bandgap of the deformed WSe_2 lattice.

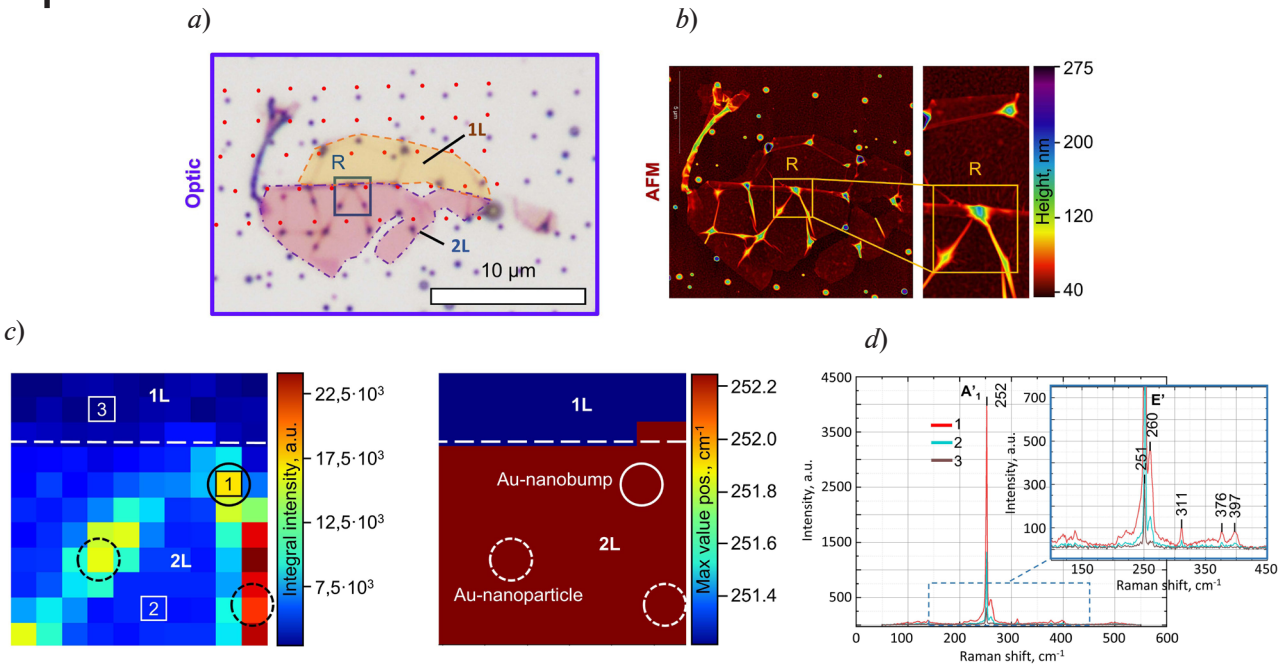

Fig. 2. WSe_2 on Au-nanobumps (29%): optical image of 1L-WSe_2 and 2L-WSe_2 flakes on Au-nanobumps indicated by red dots (*a*) and AFM-map (*b*) with the selected Raman mapping area *R*; Raman mapping of the area *R* representing integral intensity and the primary peak position of Raman spectra, in cm^{-1} (*c*); Raman spectra of the dots 1, 2 and 3 represented on the integral intensity map (*d*)

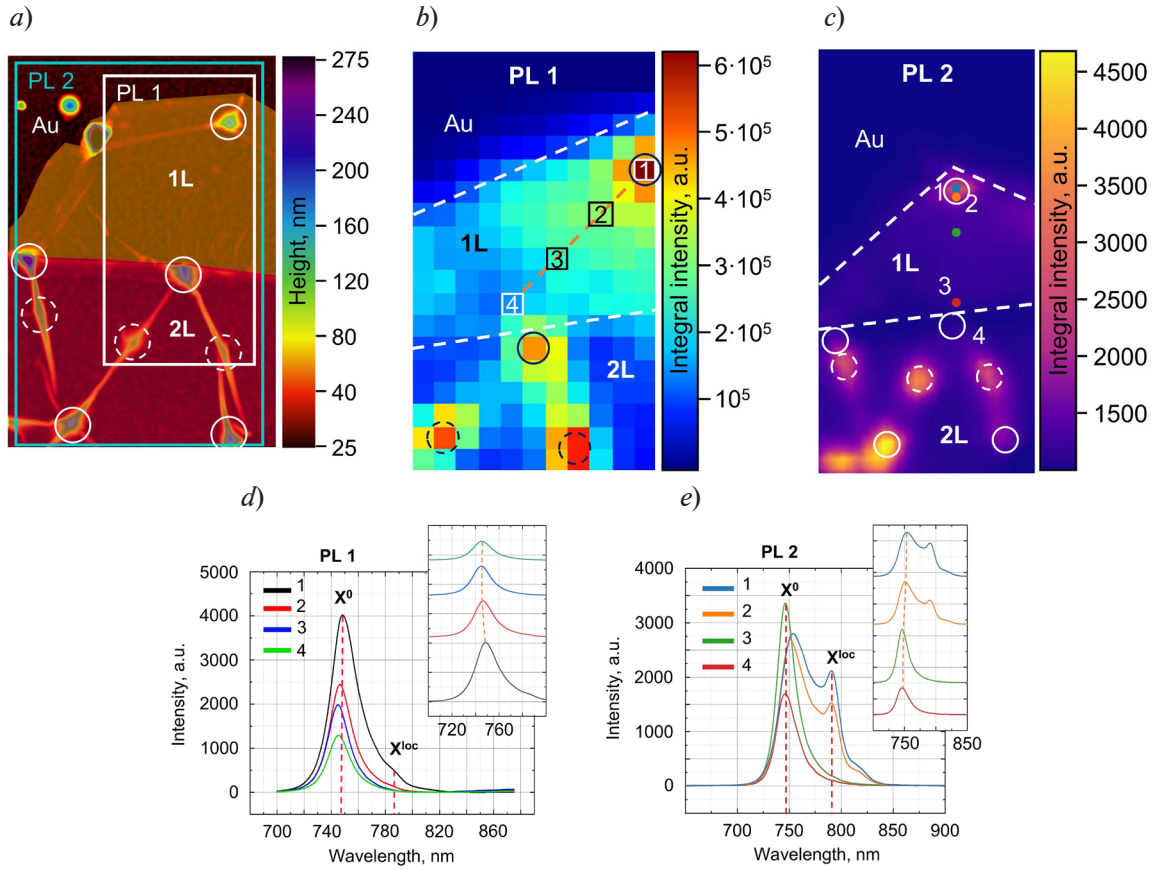

Fig. 3. AFM map (*a*) and photoluminescence map PL 1 at 532 nm (*b*) and PL 2 at 473 nm (*c*) excitation and the corresponding spectra (*d*, *e*). The locations of Au-nanobumps and Au-nanoparticles on all maps are highlighted with solid and dashed circles, respectively

The photoluminescence (PL) spectra of area 1 (Fig. 3, *d*) exhibit a low-energy shoulder at 785 nm alongside the neutral exciton X^0 peak at 750 nm. This feature can likely be attributed to a strain-localized exciton (X^{loc}) as shown in the work on WS_2 [7]. Localized excitons in transition metal dichalcogenide (TMDC) monolayers typically arise from structural defects or spatially confined strain. The concept of localized excitons is further substantiated by the ability to deterministically create nanoscale potential wells through precisely induced deformation at predefined sites, which effectively funnel excitons and give rise to strain localized excitonic states. Mapping of the same area under 473 nm laser excitation (Ntegra Spectra II system, NT-MDT) revealed a significant alteration of the spectral profile near the nanobump (Fig. 3, *e*): the low-energy state at 788 nm appears as a distinct, intense peak rather than a shoulder. Concurrently, the X^0 peak shows no enhancement. This observation can be interpreted from two perspectives: firstly, in terms of energy transfer between the two states (X^0/X^{loc}), and secondly, considering the disparity in excitation power at 532 nm (3.9 mW/μm²) versus 473 nm (5 μW/μm²). At lower power levels, the low-energy state becomes more prominent, emerging against a backdrop of diminished neutral exciton photoluminescence intensity. Moreover, the more pronounced enhancement of the neutral exciton (X^0) under 532 nm excitation can be attributed to the spectral overlap between the pump energy and the maximum of the nanobumps' plasmon resonance (Fig. 1, *c*).

To investigate this spectral feature further, low-temperature photoluminescence measurements at 10 K were performed using a customized setup. The micro-PL system for low-temperature measurements comprised a Hubner C-Wave tunable continuous-wave (CW) laser with a radiation wavelength of 512 nm. The sample was mounted in a Montana Instruments Cryostation S50 with optical access. The photoluminescence signal was collected and analyzed using a HORIBA Jobin Yvon iHR320 spectrometer equipped with a Horiba SynapsePlus detector.

Fig. 4, *a* presents the photoluminescence (PL) intensity map integrated around 1.617 eV state, acquired at 10 K. Within this selected spectral window, the integrated PL intensity reaches its maximum near the nanobump. For reference, the corresponding AFM topography is provided on the same panel, indicating the 1L-WSe_2 and 2L-WSe_2 regions, as well as the specific points of PL spectra shown in Fig. 4, *c*.

The low-temperature PL spectra of WSe_2 contain, in addition to the primary neutral exciton (X^0) and trion (X^T) states in accordance with the work [8], an ensemble of low-energy features commonly interpreted in the literature as localized excitonic states [9]. Both the neutral exciton and the trion exhibit a red shift on the nanobump compared to the flat region: 1.8 meV for X^0 and 4.3 meV for XT. The pronounced peak at 1.617 eV, corresponding to the maximum photoluminescence intensity in the deformed WSe_2 region beneath the nanobump, can be interpreted as a potential low energy strain-localized state, which is also observed in room temperature spectra.

This spectral reorganization demonstrates the pronounced effect of strain and plasmonic enhancement on the optoelectronic properties of 1L-WSe_2. It highlights the potential for actively tuning the photoluminescence in hybrid plasmonic nanostructure/2D material systems, which is highly relevant for developing nanolasers, highly sensitive sensors, and nanophotonic components.

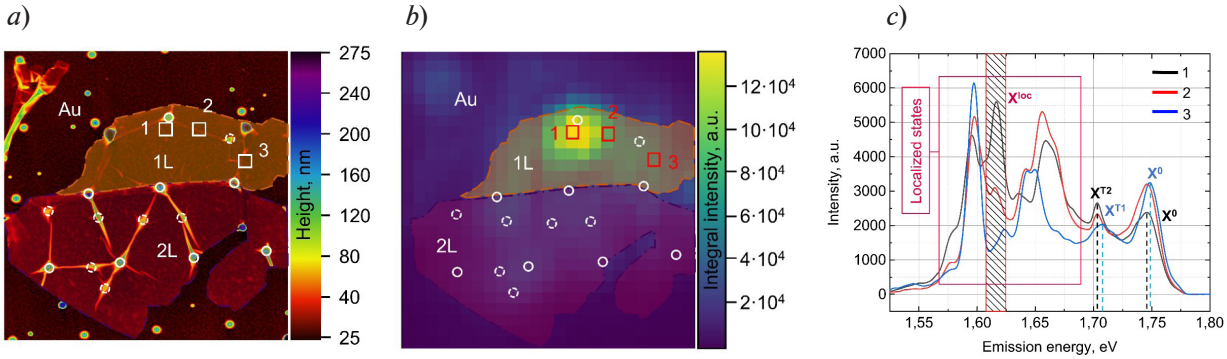

Fig. 4. AFM map (*a*) and photoluminescence map (*b*) at 10 K and 512 nm excitation and the corresponding spectra (*c*). The locations of Au-nanobumps and Au-nanoparticles on all maps are highlighted with solid and dashed circles, respectively

Conclusion

In summary, we demonstrated the integration of a WSe_2 monolayer with a plasmonic Au-nanobumps surface, fabricated via simple and cost-effective femtosecond laser printing and dry transfer. This hybrid system leverages a dual mechanism combining resonant plasmonic enhancement with strain-induced bandgap engineering. The observed pump-strain-driven spectral redistribution, characterized by a red shift and controlled correlation between intensity of neutral exciton and low-energy excitonic features, confirms the decisive role of nanoscale deformation in modulating optoelectronic properties. This study presents a versatile platform for spectrally tunable light emission, advancing the development of nanoscale light sources and strain-sensitive nanophotonic components.

Acknowledgments

A.V.N. thanks the Ministry of Science and Higher Education of the Russian Federation (Grant FSRM-2026-0004) for supporting the processing. M.A.A. thanks the Ministry of Science and Higher Education of the Russian Federation (project FSMG-2025-0005) for support of the PL mapping. A.D.B. acknowledges Saint-Petersburg State University for a research project 122040800254-4 supporting the paper preparation.

REFERENCES

1. **Kuznetsov A., Anikina M.A., Toksumakov A.N., Abramov A.N., Dremov V.V., Zavyalova E.G., Kondratev V.M., Fedorov V.V., Mukhin I.S., Kravtsov V., Novoselov K.S., Arsenin A.V., Volkov V.S., Ghazaryan D.A., Bolshakov A.D.,** In-Plane Directional MoS_2 Emitter Employing Dielectric Nanowire Cavity, Small Structures. (2025).

2. **Nikolaeva A.V., Anikina M.A., Kondratev V.M., Sharov V.A., Barulina E.Yu., Gridchin V.O., Khrebtov A.I., Kuchmizhak A.A., Bolshakov A.D.,** Hybrid emitters based on two-dimensional WSe_2 and ordered plasmonic nanobumps, St. Petersburg State Polytechnical University Journal. Physics and Mathematics. 18 (3.1) (2025) 30–35.

3. **Uymina P.G., Anikina M.A., Speshilova A.B., Kondratev V.M., Karaseva E.P., Shmakov S.V., Kuznetsov A., Syuy A.V., Osipov A.A., Mishin M.V., Bolshakov A.D.,** Blossoming layers: Morphological engineering of vertically aligned MoS_2 sheets, Materials Science in Semiconductor Processing. 200 (2025) 109906.

4. **Nikolaeva A.V., Kondratev V.M., Kadinskaya S.A., Kolesina D.E., Zubov F.I., Anikina M.A., Dvoretckaia L.N., Lendyashova V.V., Gridchin V.O., Monastyrenko A.O., Krasnikov D.V., Nasibulin A.G., Kochetkov F.M., Bolshakov A.D.,** ZnO nanowire-based flexible sensors for pressure and temperature monitoring, Materials Science in Semiconductor Processing. 189 (2025) 109253.

5. **Lapidas V., Cherepakhin A., Storozhenko D., Gurevich E.L., Zhizhchenko A., Kuchmizhak A.A., Lapidas V., Cherepakhin A., Storozhenko D., Gurevich E.L., Zhizhchenko A., Kuchmizhak A.A.,** Surface coloring and plasmonic information encryption at 50000 dpi enabled by direct femtosecond laser printing, Nano Letters. 24 (40) (2025) 12590–12596.

6. **Sergeeva K.A., Pavlov D.V., Seredin A.A., Mitsai E.V., Sergeev A.A., Modin E.B., Sokolova A.V., Tsz Chun Lau, Baryshnikova K.V., Petrov M.I., Kershaw S.V., Kuchmizhak A.A., Kam Sing Wong, Rogach A.L.,** Laser-printed plasmonic metasurface supporting bound states in the continuum enhances and shapes infrared spontaneous emission of coupled HgTe quantum dots, Advanced Functional Materials. 33 (44) (2023) 2307660.

7. **Feng S., Cong H., Kholid F.N., Zhang J., Liu X., Li Y., Liu Z., Yu T., Wang G., Mohib-Ul-Kabir M., Liu Y., Lou J., Huang J., Chen Y., Ma C., Su F., Feng M., Cao Y., Liu B., He R., Du W., Dresselhaus M.S., Yang R.,** Direct observations of the rotation and translation of anisotropic nanoparticles adsorbed at a liquid-solid interface, ACS Nano. 16 (6) (2022) 9217–9228.

8. **Robert C., Lagarde D., Cadiz F., Wang G., Lassagne B., Amand T., Balocchi A., Renucci P., Tongay S., Urbaszek B., Marie X.,** Exciton radiative lifetime in transition metal dichalcogenide monolayers, Physical Review B. 93 (20) (2016) 205423.

9. **Wang G., Bouet L., Lagarde D., Vidal M., Balocchi A., Amand T., Marie X., Urbaszek B.,** Valley dynamics probed through charged and neutral exciton emission in monolayer WSe_2, Physical Review B. 90 (7) (2014) 075413.

THE AUTHORS

NIKOLAEVA Aleksandra V.
nikalex2000@bk.ru
ORCID: 0009-0008-4344-4863

ANIKINA Maria A.
mari.a.nikina@yandex.ru
ORCID: 0000-0002-5522-5026

PAVLOV Dmitrii V.
pavlov.dim@mail.ru
ORCID: 0000-0001-8726-5615

MAKSIMOV Fedor M.
maksimov.fm@phystech.edu
ORCID: 0000-0002-2845-5061

KUZNETSOV Alexey
alkuznetsov1998@gmail.com
ORCID: 0000-0001-7143-6686

KONDRATEV Valeriy M.
kvm_96@mail.ru
ORCID: 0000-0002-3469-5897

SHAROV Vladislav A.
vl_sharov@mail.ru
ORCID: 0000-0001-9693-5748

KUCHMIZHAK Aleksandr A.
ku4mijak@iacp.dvo.ru
ORCID: 0000-0002-5376-5555

BOLSHAKOV Alexey D.
acr1235@mail.ru
ORCID: 0000-0001-7223-7232

Received 14.12.2025. Approved after reviewing 10.02.2026. Accepted 03.03.2026.